Received: 6 August 2020 | Revised: 21 December 2020 | Accepted: 17 January 2021

DOI: 10.1111/ffe.13423

ORIGINAL CONTRIBUTION

FFEMS Fatigue & Fracture of Engineering Materials & Structures WILEY

Fatigue of X65 steel in the sour corrosive environment—A novel experimentation and analysis method for predicting fatigue crack initiation life from corrosion pits

Farnoosh Farhad[1] | **David Smyth-Boyle**[2] | **Xiang Zhang**[3]

[1]Faculty of Engineering and Environment, Mechanical and Construction Engineering Department, Northumbria University, Newcastle upon Tyne, UK

[2]The Welding Institute (TWI) Ltd., Cambridge, UK

[3]Faculty of Engineering, Environment and Computing, Coventry University, Coventry, UK

Correspondence
F. Farhad, Faculty of Engineering and Environment, Mechanical and Construction Engineering Department, Wynne Jones Building, Northumbria University, Newcastle upon Tyne, NE1 8ST, UK.
Email: farnoosh.farhad@northumbria.ac.uk

Funding information
BP; The Welding Institute (TWI) Ltd.; Coventry University

Abstract

Oil and gas pipelines manufactured from API-5L Grade X65 steel are generally subjected to cyclic loading and their internal surfaces are frequently exposed to corrosive sour fluids. Exposure of pipelines to these environments often leads to localized corrosion (pitting) and decreased fatigue life. Corrosion pits are geometrical discontinuities that may promote fatigue cracking by acting as stress raisers. In order to optimize asset inspection and repair scheduling, it is important to understand the fatigue behavior of X65 steel and in particular, the ability to predict the crack initiation from corrosion pit. To achieve this level of understanding, conducting fatigue tests in an environmental condition replicating the field environment is important. This paper presents the test protocol and results of environmental fatigue testing using bespoke laboratory apparatus to undertake in situ corrosion fatigue tests in a sour corrosive environment under uniaxial loading. The environment selected represent processes that are likely to occur at internal surfaces of oil and gas pipelines exposed to production fluids. The tests were carried out on smooth samples to obtain S-N curve in this specific environment as well as on pre-pitted samples. An electrochemical method is used to create corrosion pits on the samples. Also, a model is proposed to predict the crack initiation life from corrosion pit, using a local stress-based technique, which has been validated by experimental test results. Post-test fractography was carried out by scanning electron microscopy (SEM). The performance of our approach is demonstrated. The innovation is anticipated to encourage other workers to employ similar small-scale tests requiring toxic and challenging test environments.

KEYWORDS

environmental fatigue testing, fatigue crack initiation, life prediction, oil and gas pipelines, pitting corrosion, X65 steel

1 | INTRODUCTION

API-5L Grade X65 steel are commonly used to manufacture pipelines used to convey production fluids extracted by the oil and gas industry.[1,2] The mechanical properties, cost, and availability are the main factors that determine the selection of steel. However, despite having modest resistance to uniform corrosion, this grade of steel is prone to localized corrosion (pitting) upon exposure to sour corrosive environments,[3,4] typical for many mature oil and gas reservoirs. The sour corrosive media can reduce the fatigue life of pipelines under the cyclic load[5] applied from sea waves, seabed movements, and internal pressure variation.[6] In order to increase operational safety and minimize the likelihood of pipelines failures, a better informed and more efficient maintenance and inspection schedule is required. A vital prerequisite on the path to meet these goals is the development of a more reliable fatigue life prediction model.

The presence of corrosion pits has been cited as main contributory factor in many failures of pipelines reported by the oil and gas industry.[2,3] Corrosion pits are a form of localized corrosion that can jeopardize the life of engineering assets by accelerating material loss over a small area or by increasing the risk of crack initiation as a stress riser. A major part of the total fatigue life comprises the transition of corrosion pit to fatigue cracking,[7] the so-called pit-to-fatigue crack transition that has received growing attention in recent research publications.[8] Different models exist in the literature to predict crack initiation life from corrosion pit,[9–14] which are based on linear elastic fracture mechanics (LEFM) criteria. This criterion predicts the behavior of the long crack by considering corrosion pit as a pre-existing short crack and disregards the crack initiation regime which is quite a significant regime in high cycle fatigue life. The model proposed in this paper for predicting the crack initiation life from corrosion pit in a sour environment considers pits as a stress concentration zone, that is, a notch, and predicts short crack initiation life. This model uses the data obtained from environmental fatigue testing that replicates sour conditions present in service.

Previous studies have described fatigue tests performed in air or environmental fatigue tests conducted in benign environments[10,14–17] investigating the effect of the presence of corrosion pits. In earlier publications[18,19] we have summarized the discrete parts of our initial efforts toward developing a harmonized approach to environmental fatigue testing of alloys. Prior to our work, there were no reports of small-scale corrosion fatigue tests of alloys exposed to toxic H_2S containing fluids, because of the test complexity and health and safety considerations. In this paper, we detail the overall approach for the first time and present new data concerning the effect of sour environments on fatigue behavior of materials using small-scale standard samples.

2 | EXPERIMENTAL

2.1 | Material and specimens

The material of interest in this study is seamless API-5L X65 grade pipeline steel provided by the industrial sponsor. The chemical composition was obtained by optical emission spectroscopy at The Welding Institute (TWI Ltd.) reported in previous work[20] and the cyclic and monotonic mechanical properties required in this paper were obtained from the literature[7] as reported in Table 1. The chemical composition of tested material is reported in Table 2.

All experiments were carried out on specimens extracted longitudinally from parent material of an X65 steel pipe (Figure 1A,B). The seamless pipe had an outer diameter of 273 mm and wall thickness of 29 mm. Only parent material remote from the girth weld was used in the present study. Two types of fatigue specimens were used during environmental tests, namely, smooth (Figure 1C) and pre-pitted (Figure 1D); both were designed in accordance with ASTM E466 standard. To make a smooth contact between the test apparatus o-rings and the specimen, a curved edge was used on all specimens. Initial trials indicated that, in order to decrease the number of artifacts in X-ray computed tomography images and to optimize the resolution, it was necessary to reduce the width of the pre-pitted specimens to 3 mm (Figure 1D). All test specimens were ground to a 4000 paper finish (carbon-silica) prior to a final polish using a 3-μm cloth to minimize the potential effects of residual stress and surface roughness on fatigue behavior.

2.2 | Pre-pitting of the specimens using an electrochemical cell

A number of specimens used in fatigue tests were pre-pitted using a micro-electrochemical cell constructed at TWI Ltd. The electrolyte used during these studies was 3.5% NaCl solution (exposed to ambient air). Figure 2 shows the main components of the electrochemical workstation including the electrochemical microcell and Figure 3 is a close-up view of the microcell. The cell was installed on a VersaSCAN device that allows precise

TABLE 1 Mechanical properties of API-5L-X65 used in this study[7]

Elastic modulus, E(GPa)	211
Yield strength, YS (MPa)	516
Cyclic strength coefficient, $\acute{K}$(MPa)	923
Cyclic strain hardening exponent, $\acute{n}$	0.118

TABLE 2 Chemical composition of API-5L X65 steel (mass %)

C	Si	Mn	Mo	Cr	P	Cu	S	Ni	V
0.06	0.11	1.38	0.21	0.27	0.01	0.027	0.002	0.022	0.053

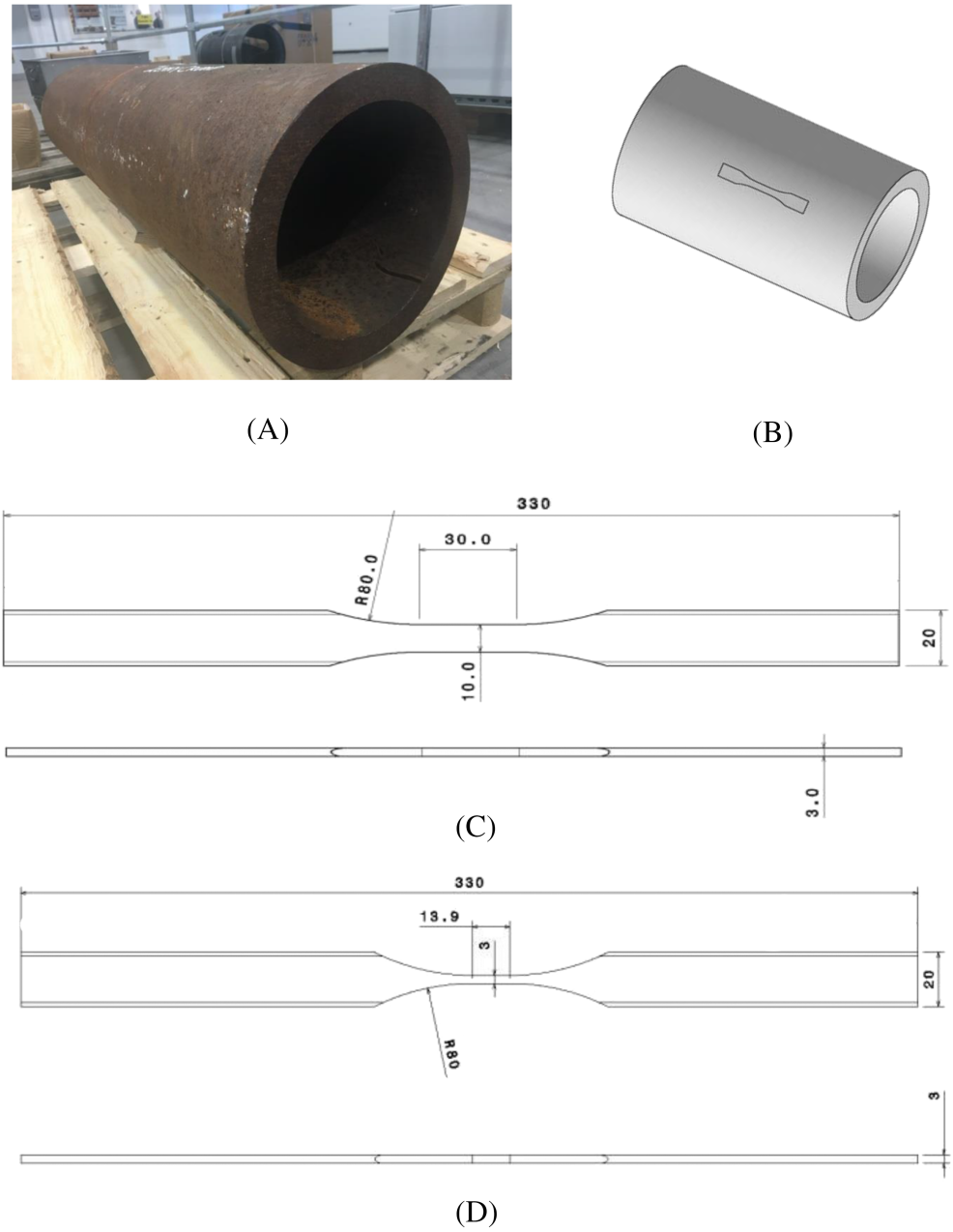

(A) (B) (C) (D)

FIGURE 1 (A) As-received X65 seamless pipe with an outer diameter of 273 mm and a wall thickness of 29 mm, (B) orientation of test specimen extraction, (C) smooth specimen for corrosion fatigue test, and (D) pre-pitted specimen for corrosion fatigue test (unit: Mm) [Colour figure can be viewed at wileyonlinelibrary.com]

positioning of the cell along three orthogonal axes. A standard three-electrode configuration (i.e., working, counter and reference electrodes) was employed, using a platinum wire as the counter electrode and an Ag/AgCl reference electrode. All the electrodes are attached to VersaSTAT 4 potentiostat-galvanostat. Both the VersaSCAN and VersaSTAT 4 were controlled using VersaStudio software and a laptop PC. The purpose of the microcell is to control the size of the wetted area of the specimen surface, by using a micro-capillary to form a droplet that can be positioned on the specimen surface and thus impart region-selectivity to the electrochemical corrosion process. A video camera accessory is used to accurately position and monitor the droplet at the specimen surface prior to and during the electrochemical corrosion (i.e., pitting) process. Figure 4 shows a close-up view of a pre-pitted specimen. Following polarization, the specimens were placed in a Pyrex glass beaker containing acetone and cleaned by ultrasonication. The as-grown pits were characterized using an Alicona Laser Scanning

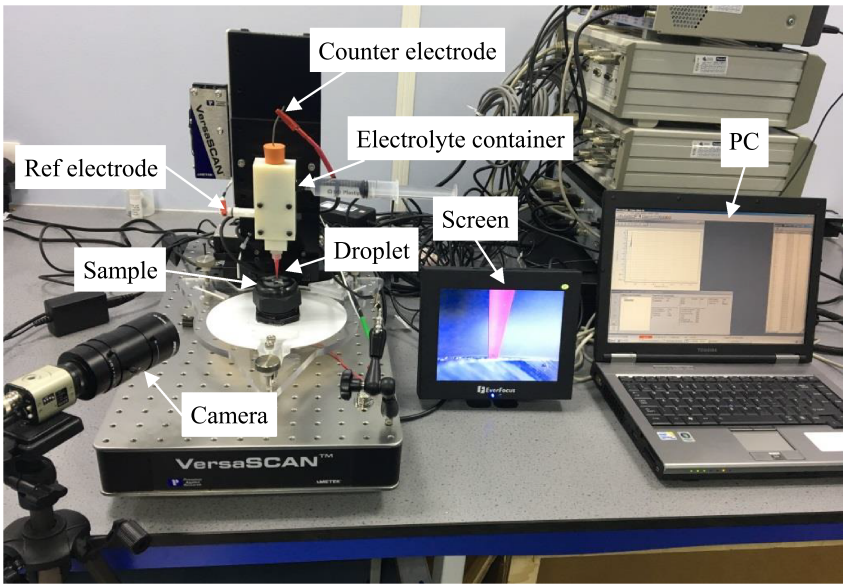

FIGURE 2 Overview of the micro-electrochemical apparatus used to create the corrosion pits [Colour figure can be viewed at wileyonlinelibrary.com]

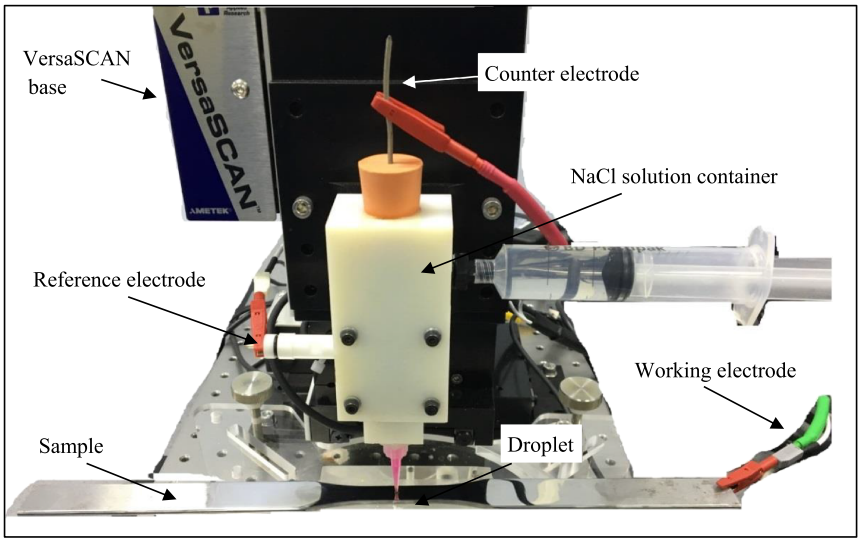

FIGURE 3 Close-up view of the electrochemical micro-capillary cell used to create a single corrosion pit [Colour figure can be viewed at wileyonlinelibrary.com]

FIGURE 4 Close-up view of a pre-pitted specimen. The pit width (diameter) is 520 μm and pit depth is 174 μm [Colour figure can be viewed at wileyonlinelibrary.com]

Confocal Microscope with resolution of 0.1 micron. The pit depth and lateral dimensions were recorded across four directions as shown in Figure 5A. The average of the measured values for the four profiles was used to define the final depth and width of pits. A representative confocal microscopy scan and a 2D-cross-sectional profile are shown in Figure 5B,C, respectively.

The pits generated using this method are morphologically similar to the pits seen on the internal surface of the pipes; in terms of pit depth, width and cross-sectional shapes of corrosion pits as observed in samples and data (i.e., data collected using non-destructive testing (NDT) methods on steel production risers) provided by the industrial sponsor of this project.

2.3 | In situ corrosion fatigue test apparatus

A bespoke environmental apparatus was developed to facilitate the environmental tests and visualize the

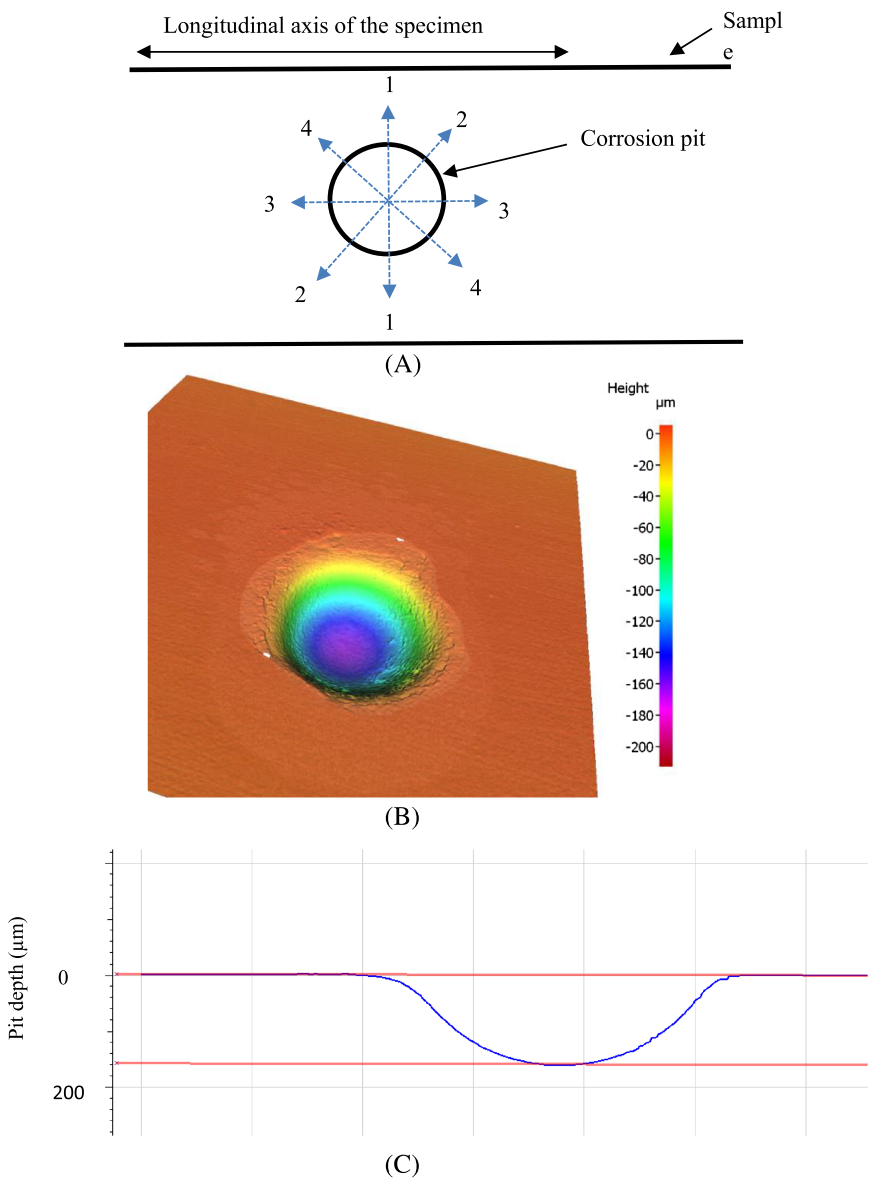

FIGURE 5 (A) Schematic showing the directions of each profile taken from confocal microscopy scan to measure the pit depth and pit width; (B) confocal microscopy scan of a pit. (C) a profile taken from confocal microscopy of a pit for measuring pit depth [Colour figure can be viewed at wileyonlinelibrary.com]

initiation of a fatigue crack from a corrosion pit in X65 steel using X-ray CT. The development of the apparatus including material and size selection is detailed in previous work.[18] The provision of robust sealing for the test cell was a vital consideration, due to the toxic nature of the H_2S contained therein and the need to exclude oxygen from the test environment. The configuration employed in this work ensured that the contents of the cell were fully isolated from the external environment throughout testing using axially loaded small-scale tensile specimens. The overall height of the vessel was chosen to be 130 mm to accommodate the specimen dimensional requirements stated in ASTM E466. The specimen's dimensions are stated in Section 2.1 and Figure 1. Figure 6 shows the vessel placed inside the fatigue test machine. The gas/solution inlets and outlets are also shown.

2.4 | Fatigue test procedure in the sour environment

A corrosion pit of the desired dimensions was created in the center of the test section of the specimen by using the electrochemical cell (see Section 2.2). Table 3 shows the size of corrosion pits of the 10 specimens for corrosion fatigue test. An initial corrosion fatigue test was performed using the smooth specimen to both check the performance of the apparatus and also to obtain an estimate of the number of cycles to failure in a corrosive environment. The specimens were tested under the constant amplitude loading condition and sinusoidal waveform in the high cycle fatigue regime. The applied stress ratio (R) was 0.1 for all tests. The applied stress amplitude ranged from 135 to 225 MPa (corresponding maximum applied stress from 300 to 500 MPa) for the 10 smooth specimens

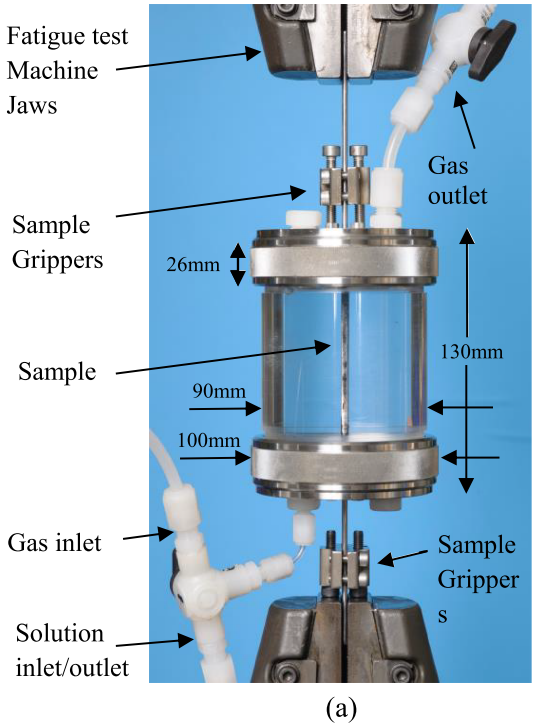

FIGURE 6 The corrosion fatigue test apparatus mounted in the fatigue test machine showing the inlets and outlets of gas and solution and key dimensions[18] [Colour figure can be viewed at wileyonlinelibrary.com]

with cross-sectional area of 3 × 10 mm^2 (Figure 1C). The 10 pre-pitted specimens with cross-sectional area 3 × 3 mm^2 (Figure 1D) were tested at two different applied stress amplitudes of 165 and 185 MPa, corresponding to maximum applied stress 367 MPa (~70% YS) and 412 MPa (~80% YS), respectively, at the gauge section. The yield strength is 516 MPa. Table 3 shows the applied stress amplitudes for the pre-pitted samples. A frequency of 0.3 Hz was applied in order to allow the corrosive environment to interact with the specimen. Testing was conducted at ambient pressure and temperature. The test environment comprised 3.5% w/v NaCl solution saturated with a gas mixture containing 12.5% H_2S in CO_2 balance.

The sour corrosion fatigue tests were performed in the Gooch laboratory at TWI Ltd. in Cambridge, which has fixed H_2S sensors for monitoring and suitable extraction and safety procedures in place. Prior to starting the test, 3.5% NaCl solution was deaerated by purging with high-purity nitrogen for 24 h in a sealed High-Density Polyethylene (HDPE) barrel. Previous work at TWI Ltd. has shown that this process reduces the measured dissolved oxygen content to below 10 ppb.[20] For each test, once the apparatus and specimen were assembled and placed in the fatigue loading machine, a leak test was carried out by pressurizing the test cell with nitrogen to 0.5 barg to ensure that the seals did not leak. Following confirmation of seal integrity, the test cell was deaerated using a fast purge of nitrogen for 1 h, then charged with 3.5% NaCl solution, and then purged once again with nitrogen for approximately 1 h. Upon completion of this process, the test solution in the cell was saturated with sour test gas (i.e., containing 12.5% H_2S) using a fast purge for 1 h. Finally, the fatigue load was applied to the specimen. The vessel contains about 380 cm^3 of the solution. The experimental setup is reported in previous work.[18]

3 | RESULTS AND DISCUSSIONS

3.1 | Environmental fatigue testing on smooth and pre-pitted samples

Using the test protocol described in Section 2.4, in situ corrosion fatigue tests were carried out on 10 smooth

TABLE 3 Corrosion pit size of pre-pitted specimens (unit: μm)

Specimen code	Pit depth, *a*	Pit width, 2*c*	Aspect ratio, *a*/2*c*	Applied stress amplitude (MPa)
F01	154	534	0.29	165
F02	289	642	0.45	165
F03	231	580	0.40	186
F04	245	597	0.41	186
F05	303	700	0.43	186
F06	312	590	0.53	186
F07	308	584	0.53	165
F08	271	512	0.53	165
F09	167	503	0.33	165
F10	173	487	0.35	186

specimens to obtain S-N data in the sour environment. The results are plotted in Figure 7. The fatigue test carried out in air on X65 steel in authors' previous work is described in full in previous work.[21] It can be seen that in the sour environment, a significant reduction in fatigue strength is apparent for all stress levels investigated in comparison to the corresponding fatigue strength tested in the air. The best fitted trend line for experimental data with regression of $R^2 = 0.78$ was obtained using a power law type equation that is displayed on the graph. Other types of functions showed R^2 being 0.62 for exponential, 0.59 for linear, and 0.71 for polynomial relations. Interestingly, comparison of the best fitted sour environment S-N curve with the one obtained in the air condition indicates that the fatigue strength reduction was more significant at higher fatigue lives. This finding is consistent with literature studies in this area where a corrosive environment was shown to reduce fatigue life more significantly at lower stress amplitudes.[22,23] This happens because at lower stress amplitudes, the environment has more time to interact with the material and in the case of sour environments, ingress of embrittling atomic hydrogen is anticipated. The Basquin equation for sour environment S-N curve that is obtained from the best fitted line with the test data is

$$\sigma_a = 1179.5\left(N_f\right)^{-0.161} \quad (1)$$

where σ_a is the applied stress amplitude and N_f is the number of cycles to failure, at $R = 0.1$. This empirical equation calibrated on this first set of results was used for the life prediction of pre-pitted specimens reported in the later section.

Figure 7 also shows the environmental fatigue tests on pre-pitted specimens described in Table 3 at two different stress amplitudes, 165 MPa and 185 MPa. The results are compared with the smooth specimens tested in the same sour environment as well as in the air. This figure shows lower fatigue strength of pre-pitted samples compared to the smooth samples tested in sour environment that emphasizes the effect of corrosion pits in lowering the fatigue strength as a stress raiser.

Previous work by the authors has shown the initiation of fatigue crack from corrosion pits in pre-pitted samples, captured by X-ray tomography by interrupting the environmental fatigue tests.[18] It was observed that crack initiation life, N_i, was about 90% of the total number of cycles to final failure, N_f. Therefore, on consideration of this observation and also the small thickness of the fatigue test specimens, N_i in this paper is approximated as 90% N_f.

To study the effects of applied stress, pit geometry and pit size on fatigue crack initiation life, Murakami's square-root-area parameter model was used in

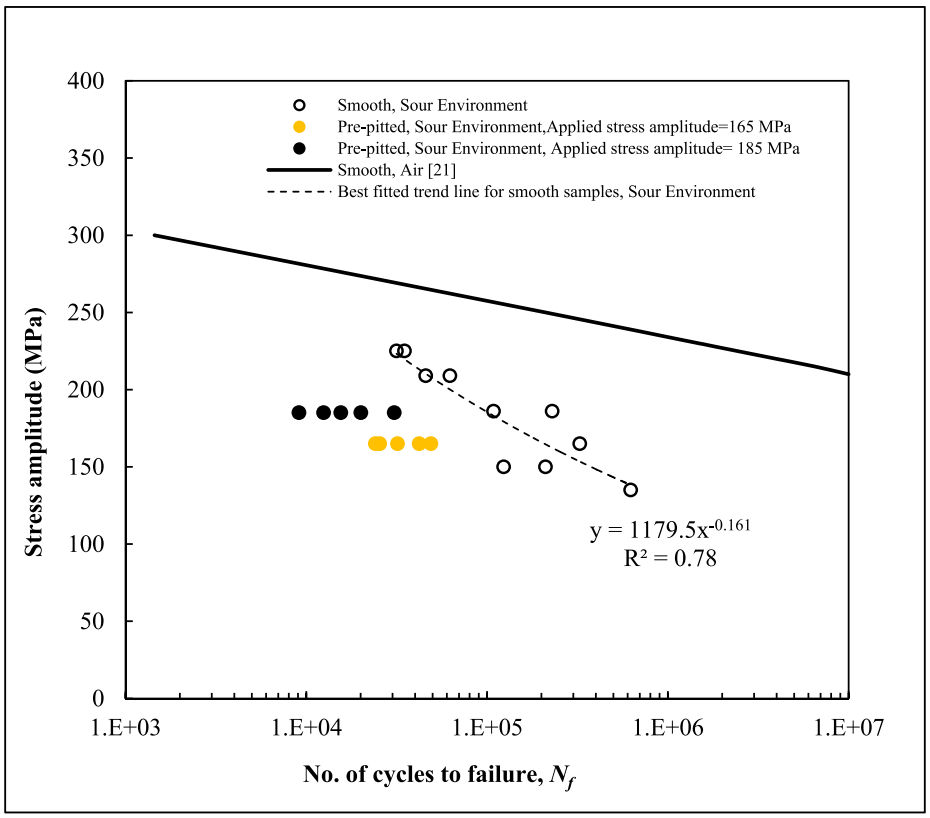

FIGURE 7 Stress versus number of load cycles to failure for X65 steel tested at $R = 0.1$ in the air and sour environment (smooth and pre-pitted specimens) [Colour figure can be viewed at wileyonlinelibrary.com]

calculating the stress intensity factor range, that is, using Equation 2[24,25]:

$$\Delta K = 0.65\,\Delta S\sqrt{\pi\sqrt{area}} \quad , \quad area = \pi c^2 \tag{2}$$

where ΔS is the applied stress range and c is half of the pit mouth width, that is, pit mouth radius.

Figure 8 shows the relation between the stress intensity factor range and crack initiation life. A good correlation is established for all test data covering two different applied stress levels and a range of pit geometry and sizes as given in Table 3. This is because that the stress intensity factor takes account of both the applied cyclic stress and the pit size.

This result is rather significant in the context of fatigue data collected in sour corrosive environments and, in addition, obtained using small scale coupon samples for the first-time.

3.2 | Prediction model for crack initiation life from corrosion pit

The notch stress approach was used to predict the crack initiation life of the pre-pitted specimens tested in the sour corrosive environment. First, the local stress amplitude at corrosion pits was calculated by Glinka's formula (Equation 3)[26,27] where ΔS and $\Delta\sigma$ are applied and local stress range, E the elastic modulus, $\acute{n}$ the cyclic strain hardening exponent, and $\acute{K}$ the cyclic strength coefficient. The required material properties in these equations are reported in Table 1. The required stress concentration factor, K_t, was calculated using Equation 4.[28] Good agreement was found between the notch stress approach and authors' finite element analysis.[19,21] In previous literature,[20] it is also shown that the pit local stress ratio obtained from Glinka's formula, at applied stress amplitude of 165 MPa and higher, is very close to the one obtained by FEA.

$$\frac{\Delta\sigma^2}{E} + \frac{4\Delta\sigma}{n'+1}\left(\frac{\Delta\sigma}{2K'}\right)^{(1/n')} = \frac{(K_t.\Delta S)^2}{E} \tag{3}$$

$$K_t = 1 + 1.25\sqrt{\frac{2}{1+\left(\frac{c}{a}\right)^2}} \tag{4}$$

Thereafter, the obtained local stress amplitude was used to predict the fatigue crack initiation life (N_i) using the material's S-N data measured in the sour environment as presented in Figure 7 and Equation 1 (i.e., by substituting the obtained local stress amplitude in Equation 1, N_f was calculated that is approximated as N_i for prediction model). The function for the prediction line in Figure 9 is then equal to Equation 1. In this work the crack initiation stage is considered as the initiation of a short crack with length of the order of 1 mm. The predicted life is shown in Figure 9 in terms of the pit local stress amplitude calculated by the aforementioned notch stress method. The experimental results of pre-pitted samples are also shown in this

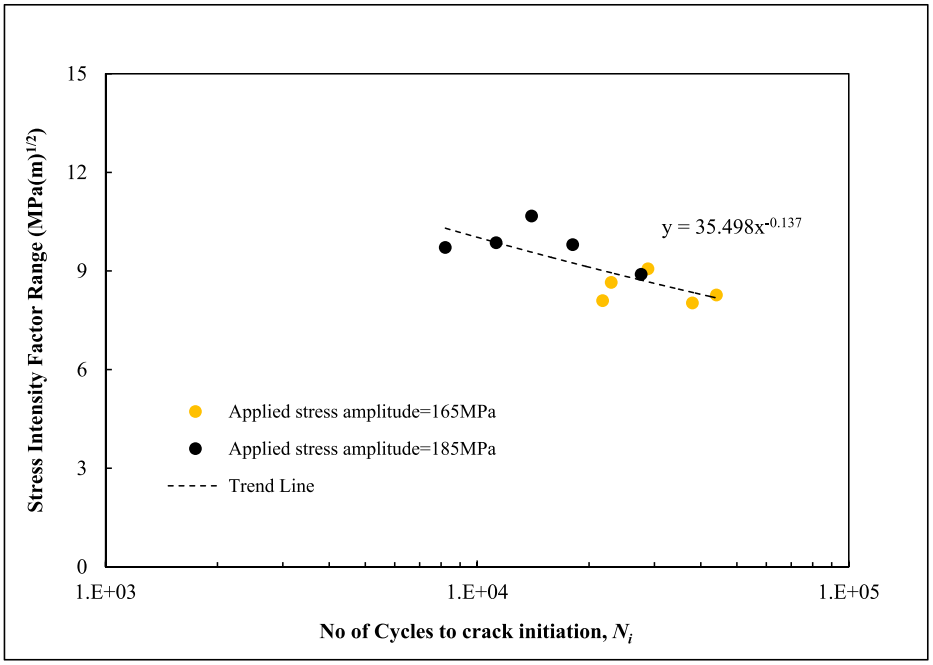

FIGURE 8 Stress intensity factor range versus number of cycles to crack initiation for pre-pitted samples tested in this study [Colour figure can be viewed at wileyonlinelibrary.com]

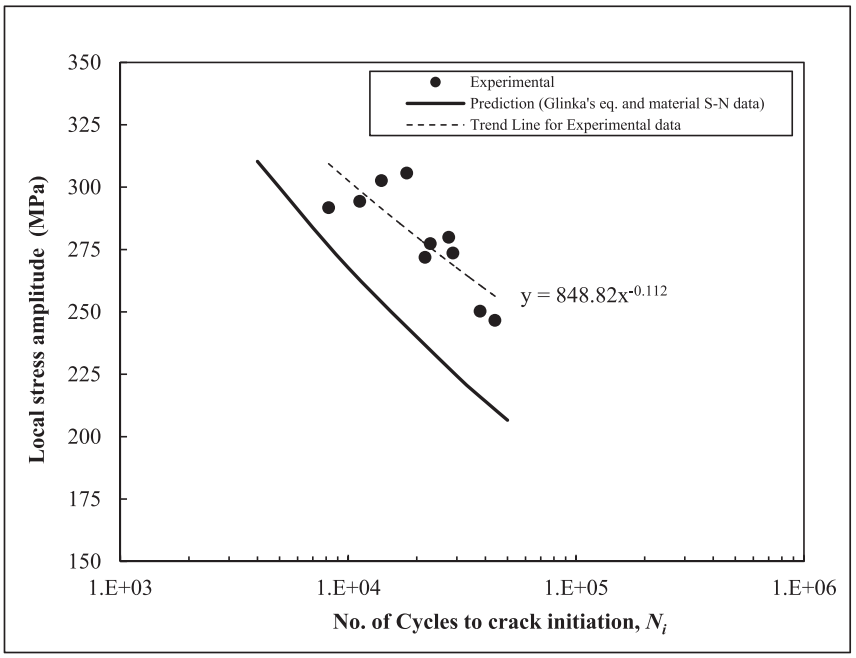

FIGURE 9 Comparison of predicted crack initiation life with the experimental test in the sour environment (pre-pitted specimens); the prediction is made in terms of the pit local stress calculated by the notch stress method, equation 3

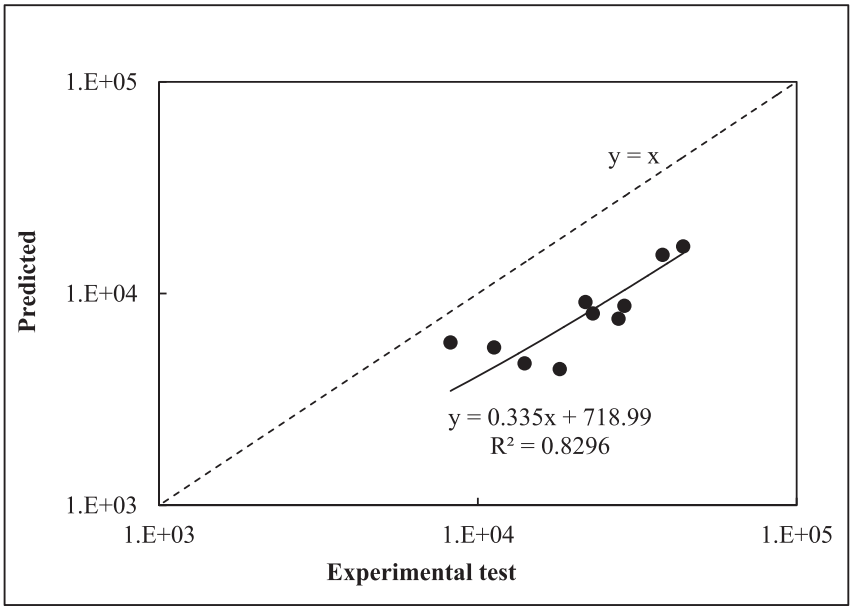

FIGURE 10 Comparison of experiment with prediction in terms of the number of cycles to crack initiation

figure in terms of local stress amplitude at the pits. It can be seen that the prediction is in a good agreement with the experimental test results. For a given life of experimental data, the relative error in local stress amplitude is between 7% and 22% with the mean difference of 16% and standard deviation of 13 MPa. The trend line in Figure 9 is obtained from best fitted line with experimental data and has a power type function with highest possible regression of $R^2 = 0.67$. Figure 10 shows number of cycles from experiments versus prediction. The envelope of data in this figure is on the conservative side, that is, right side of the $y = x$ graph. This shows that proposed prediction model does not overestimate the crack initiation life in sour environment. The predicted life is shorter than test measured; that is, prediction is conservative.

Overall, these results indicate the dependency of crack initiation life on the pit geometry and applied stress for X65 steel exposed to a sour corrosive environment. The comparison of the prediction with

experimental data provides good evidence that the proposed method for predicting the life of crack initiation from corrosion pit is a deterministic approach for X65 steel in the sour corrosive environment.

3.3 | Qualitative fractography

Following specimen failure, a fractographic analysis was undertaken using scanning electron microscopy (SEM). The purpose of fractography in this work was to understand the possible crack initiation region in the corrosion pit, that is, whether it is from the mouth of the pit or from the wall, and the predominant crack growth direction. Previous research on crack initiation life from corrosion pit of three NiCrMoV steel using X-ray microtomography confirmed that the crack initiated from the pit mouth and grew in the longitudinal direction.[29] If this is the case in X65 steel pipes in sour environment, it can cause removal of the material from the surface rather than through thickness crack growth and rupture of the pipes.

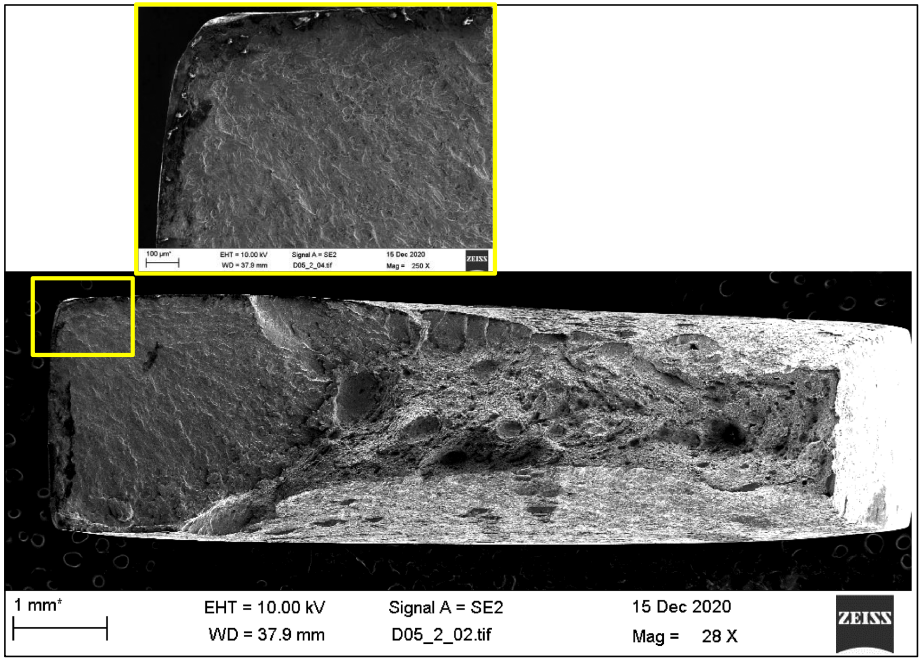

(A)

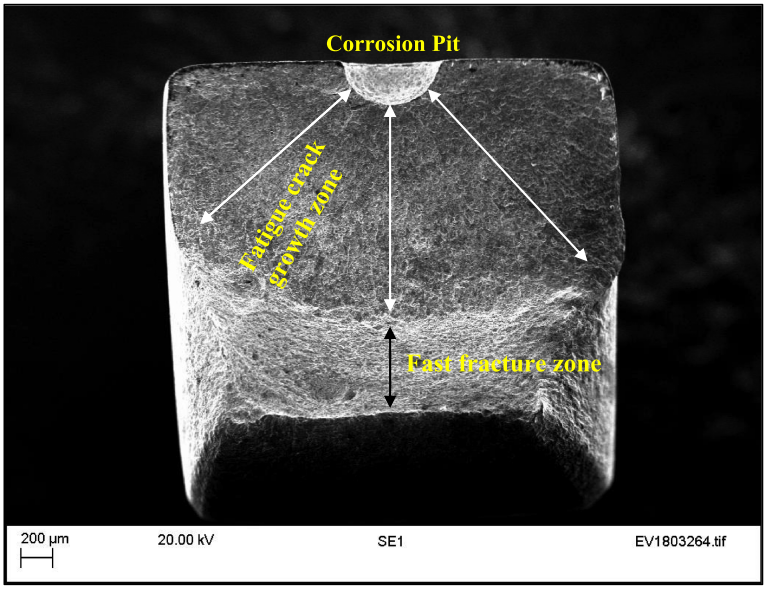

(B)

FIGURE 11 Scanning electron microscopy (SEM) images of typical fractured specimen surfaces tested in the sour environment: (A) smooth sample and (B) pre-pitted sample [Colour figure can be viewed at wileyonlinelibrary.com]

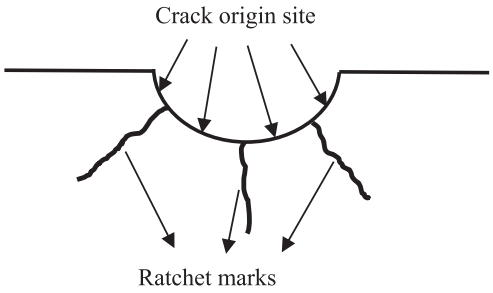

(A)

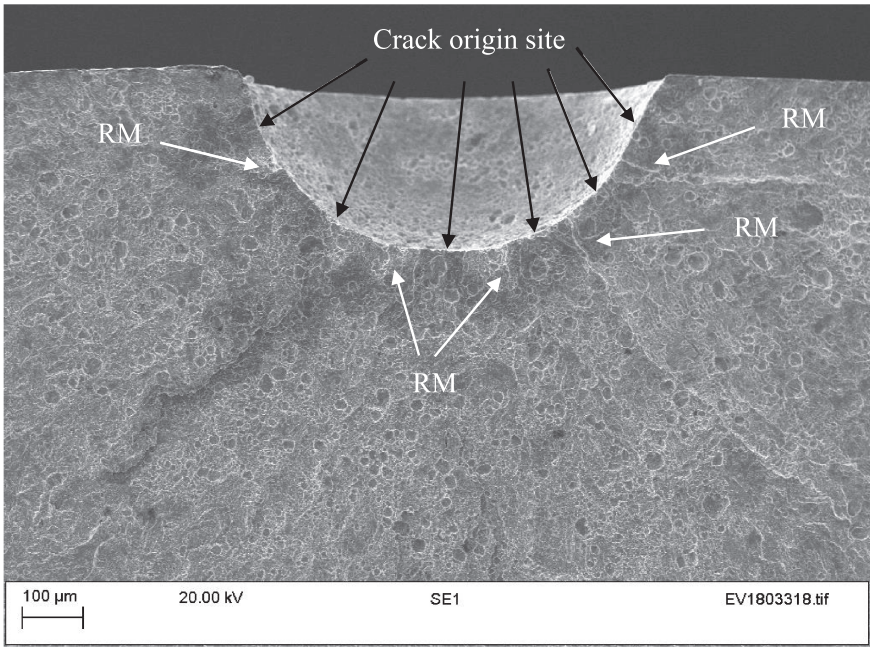

(B)

FIGURE 12 (A) Ratchet marks (RM) and crack initiation sites, after Sachs.[30] (B) Scanning electron microscopy image showing the RM and crack origins in specimen F05 tested at applied stress amplitude of 185 MPa, $N_f = 15{,}576$ cycles

Prior to microscopy, specimens were cleaned by ultrasonication in deionized water and a commercial reagent (Pyrene) to remove any surface contamination. Figure 11 provides an overview of the main surface features observed for fractured specimens. Features include the crack origin (nucleation site), ratchet marks, fatigue crack propagation, and fast fracture zones. Figure 11A shows that crack was initiated from the corner of smooth samples tested in sour environment. Corrosion pits or other stress raisers cannot be seen in the crack initiation region.

In all case, crack originated at the corrosion pit and subsequently propagated across the fatigue crack growth zone. The absence of crack growth marks (beach marks) in this zone demonstrates that there was no variation in the applied stress during tests. The plane of the fatigue crack growth zone was developed perpendicular to the plane of applied stress. Finally, cracks developed and grew to a point where brittle fracture can occur in the fast fracture zone resulting in rapid crack propagation. Another surface feature that is commonly found in fatigue failures is the ratchet marks, which represent the coalescence boundary between two adjacent cracks initiated on different geometric planes. An example of ratchet marks between two crack initiation sites is given in Figure 12A.[30]

Figure 12B show the ratchet marks and crack origin for specimen tested at stress amplitude of 186 MPa. As can be seen, there are multiple crack nucleation sites around the pit. SEM images of other specimen fracture surfaces reveal the same pattern of damage with crack origins around the corrosion pits. The SEM images from the top view of the specimens (the view of the sample shown in Figure 4) show that other cracks are initiated independent of the primary crack at the corrosion pit in other geometric planes close to the center of the pit (Figure 13). However, these features are not dominant cracks and did not contribute directly to the final failure.

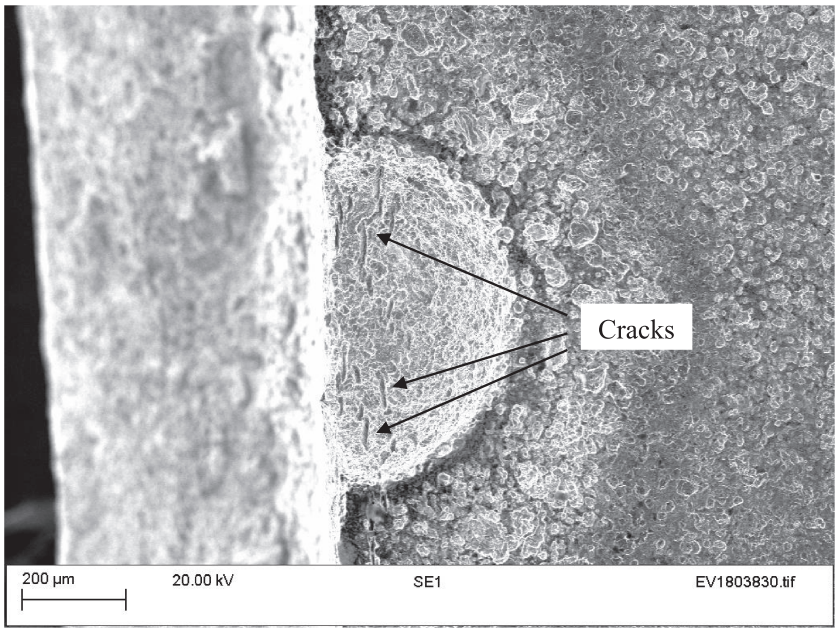

(A)

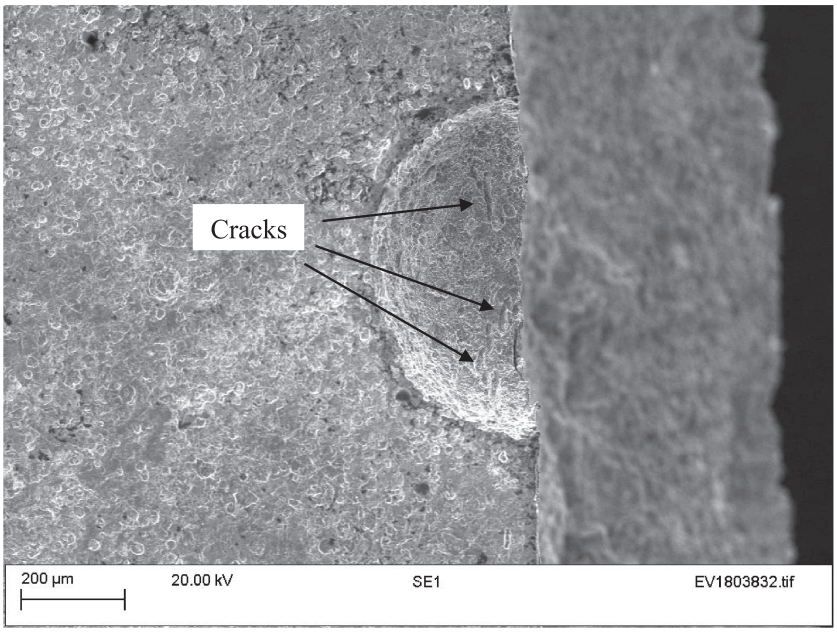

(B)

FIGURE 13 Scanning electron microscopy (SEM) images from the top view of specimen F04 showing non-propagating cracks in the right half (a), and the corresponding left half (B) of the failed specimen

4 | CONCLUSIONS

The objectives of this work were to assess the effect of a sour corrosive environment, representing typical in-service conditions of oil and gas pipes, on the fatigue crack initiation life from corrosion pit for X65 steel and to develop a predictive method for the crack initiation life. Environmental fatigue testing was carried out on small-scale coupon samples using a bespoke testing apparatus at two different stress amplitudes, 165 and 185 MPa, and 0.3 Hz frequency. The test environment comprised 3.5% w/v NaCl solution saturated with a gas mixture containing 12.5% H_2S in CO_2 balance. This study has produced an environmental S-N curve for the material and proposed a validated predictive model based on the notch stress approach. Key findings are as follows:

- A correlation was found between the crack initiation life and the pit in service conditions (i.e., pit geometry, pit mouth width, applied stress, and test environment).

- The average difference between the predicted life and experimental test result was about 16% and the prediction was on the conservative side.
- Fractography examination confirms that there were multiple crack nucleation sites around the pit. Secondary cracks also initiated independent of the primary crack at the corrosion pit in other geometric planes close to the center of the pit. However, these features were not dominant cracks and did not contribute directly to the final failure.

These findings have significant implications for the understanding of crack initiation life from corrosion pit. This work presents the first effort toward developing a harmonized approach to environmental fatigue testing of alloys, through an iterative procedure including modeling and small-scale testing. This approach will prove useful in expanding this testing protocol for other harsh environmental fatigue testing and the predictive model certainly can be used for other materials. Presumably, this method can be used for different alloys exposed to sour and other hydrogen charging conditions. There are also no obvious barriers to its application across other environmental fatigue systems where pitting is anticipated under similar cyclic loading state. It should be noted that the pre-pitting method proposed in this work should be developed according to each specific application to ensure achieving similar pit shape and sizes as in-service condition for each application.

ACKNOWLEDGEMENT

The first author would like to thank BP, TWI Ltd., and Coventry University for the sponsorship of this project. The work was enabled through, and undertaken at, the National Structural Integrity Research Centre (NSIRC), a postgraduate engineering facility for industry-led research into structural integrity established and managed by TWI Ltd. through a network of both national and international Universities. We also acknowledge Dr. Abdul Khadar Syed for his help with SEM images.

DATA AVAILABILITY STATEMENT

Data from this research will be available upon request from corresponding author.

NOMENCLATURE

a	pit depth
c	half of pit width
$a/2c$	pit aspect ratio
E	elastic modulus
$\acute{K}$	cyclic strength coefficient
K_t	stress concentration factor
N_f	number of cycles to failure
N_i	number of cycles to crack initiation
$\acute{n}$	cyclic strain hardening exponent
YS	yield strength
ΔK	stress intensity factor range
ΔS, $\Delta\sigma$	applied and local stress range
σ_a	applied stress amplitude

ORCID

Farnoosh Farhad https://orcid.org/0000-0003-1757-6834
David Smyth-Boyle https://orcid.org/0000-0002-4082-4587
Xiang Zhang https://orcid.org/0000-0001-8454-3931

REFERENCES

1. Kristoffersen M, Børvik T, Langseth M, Hopperstad OS. Dynamic versus quasi-static loading of X65 offshore steel pipes. The European physical journal special topics. Springer. 2016; 225(2):325-334.
2. Zhang G, Cheng Y. Localized corrosion of carbon steel in a CO2-saturated oilfield formation water. *Electrochimica Acta Elsevier*. 2011;56(3):1676-1685.
3. Mohammed S, Hua Y, Barker R, Neville A. Investigating pitting in X65 carbon steel using potentiostatic polarisation. *Applied Surface Science Elsevier*. 2017;423:25-32.
4. Ossai CI, Boswell B, Davies IJ. Pipeline failures in corrosive environments—a conceptual analysis of trends and effects. *Engineering Failure Analysis Elsevier*. 2015;53:36-58.
5. Srivatsan S, Sudarshan T. Mechanisms of fatigue crack initiation in metals: role of aqueous environments. *Journal of materials science. Springer*. 1988;23(5):1521-1533.
6. Zhang Y, Fan M, Xiao Z, Zhang W. Fatigue analysis on offshore pipelines with embedded cracks. *Ocean Engineering Elsevier*. 2016;117:45-56.
7. Fatoba O, Akid R. Low cycle fatigue behaviour of API 5L X65 pipeline steel at room temperature. *Procedia Engineering Elsevier*. 2014;74:279-286.
8. Larrosa N, Akid R, Ainsworth R. Corrosion-fatigue: a review of damage tolerance models. *Int Mater RevTaylor \& Francis*. 2018;63(5):283-308.
9. Goswami T, Hoeppner D. Review of pit nucleation, growth and pitting corrosion fatigue mechanisms. *Journal of the Mechanical Behavior of MaterialsDe Gruyter*. 1997;8(2):169-196.
10. Arriscorreta CA. Statistical modeling for the corrosion fatigue of aluminum alloys 7075-T6 and 2024-T3. The University of Utah; 2012.
11. Kondo Y. Prediction of fatigue crack initiation life based on pit growth. *Corrosion*. 1989;45(1):7-11.
12. Chen G, Wan K-C, Gao M, Wei R, Flournoy T. Transition from pitting to fatigue crack growth—modeling of corrosion fatigue crack nucleation in a 2024-T3 aluminum alloy. *Materials Science and Engineering: A Elsevier*. 1996;219(1–2): 126-132. https://doi.org/10.1016/S0921-5093(96)10414-7
13. Sriraman M. Pidaparti R. Crack initiation life of materials under combined pitting corrosion and cyclic loading. *Journal of materials engineering and performance. Springer*. 2010; 19(1):7-12.

14. Li S-X, Akid R. Corrosion fatigue life prediction of a steel shaft material in seawater. *Engineering Failure Analysis Elsevier*. 2013;34:324-334.
15. Baragetti S. Notch corrosion fatigue behavior of Ti-6Al-4V. *Materials Multidisciplinary Digital Publishing Institute*. 2014; 7(6):4349-4366.
16. Akid R, Dmytrakh I. Influence of surface deformation and electrochemical variables on corrosion and corrosion fatigue crack development. *Fatigue & Fracture of Engineering Materials & Structures (Print)*. 1998;21(7):903-911.
17. Wang Y, Akid R. Role of nonmetallic inclusions in fatigue, pitting, and corrosion fatigue. *Corrosion*. 1996;52(2):92-102.
18. Farhad F, Smyth-Boyle D, Zhang X, Wallis I, Panggabean D. Laboratory apparatus for in-situ corrosion fatigue testing and characterisation of fatigue cracks using X-ray micro-computed tomography. *Fatigue & Fracture of Engineering Materials & StructuresWiley Online Library*. 2018;41(12):2629-2637.
19. Hashim M, Farhad F, Smyth-Boyle D, Akid R, Zhang X, Withers PJ. Behavior of 316L stainless steel containing corrosion pits under cyclic loading. *Materials and Corrosion Wiley Online Library*. 2019;70(11):2009-2019.
20. Solving technical challenges to test in de-aerated seawater [Internet]. [cited 2020 15–12]. Available from: https://www.twi-global.com/media-and-events/insights/solving-technical-challenges-to-test-in-de-aerated-seawater
21. Farhad F, Zhang X, Smyth-Boyle D. Fatigue behaviour of corrosion pits in X65 steel pipelinesProceedings of the Institution of Mechanical Engineers, Part C. *Journal of Mechanical Engineering Science. SAGE Publications SAGEUK: London, England*. 2019;233(5):1771-1782.
22. Chlistovsky R, Heffernan P, DuQuesnay D. Corrosion-fatigue behaviour of 7075-T651 aluminum alloy subjected to periodic overloads. *International Journal of Fatigue Elsevier*. 2007; 29(9–11):1941-1949.
23. Goto M, Nisitani H. Crack initiation and propagation behaviour of a heat-treated carbon steel in corrosion fatigue. Fatigue & Fracture of Engineering Materials & Structures Wiley Online. *Library*. 1992;15(4):353-363.
24. Metal Fatigue MY. *Effects of Small Defects and Nonmetallic Inclusions*. Academic Press; 2019.
25. Murakami Y. Effects of small defects and nonmetallic inclusions on the fatigue strength of metals. JSME International Journal Ser 1, Solid Mechanics. *Strength of Materials the Japan Society of Mechanical Engineers*. 1989;32(2):167-180.
26. Glinka G. Calculation of inelastic notch-tip strain-stress histories under cyclic loading. *Engineering Fracture Mechanics Elsevier*. 1985;22(5):839-854.
27. Stephens RI, Fatemi A, Stephens RR, Fuchs HO. *Metal Fatigue in Engineering*. John Wiley & Sons; 2000.
28. Ahn S-H, Lawrence FV Jr, Metzger MM. Corrosion fatigue of an HSLA steel. Fatigue & Fracture of Engineering Materials & Structures Wiley Online. *Library*. 1992;15(7):625-642.
29. Horner D, Connolly B, Zhou S, Crocker L, Turnbull A. Novel images of the evolution of stress corrosion cracks from corrosion pits. *Corrosion Science Elsevier*. 2011;53(11):3466-3485.
30. Sachs NW. Understanding the surface features of fatigue fractures: how they describe the failure cause and the failure history. *Journal of failure analysis and prevention. Springer*. 2005;5(2):11-15.

How to cite this article: Farhad F, Smyth-Boyle D, Zhang X. Fatigue of X65 steel in the sour corrosive environment—A novel experimentation and analysis method for predicting fatigue crack initiation life from corrosion pits. *Fatigue Fract Eng Mater Struct*. 2021;44:1195–1208. https://doi.org/10.1111/ffe.13423